Genetics in Medicine (2024) 26, 101097

ELSEVIER

Genetics in Medicine
An Official Journal of the ACMG

www.journals.elsevier.com/genetics-in-medicine

BRIEF REPORT

# Biallelic loss-of-function variants of *SLC12A9* cause lysosome dysfunction and a syndromic neurodevelopmental disorder

Andrea Accogli[1,2], Young N. Park[3], Guy M. Lenk[3], Mariasavina Severino[4], Marcello Scala[5,6], Jonas Denecke[7], Maja Hempel[8], Davor Lessel[8], Fanny Kortüm[8], Vincenzo Salpietro[9,10], Patrizia de Marco[11], Sara Guerrisi[11], Annalaura Torella[12,13], Vincenzo Nigro[12,13], Myriam Srour[2,14,15,16], Ernest Turro[17,18,19], Veerle Labarque[20,21], Kathleen Freson[20], Gianluca Piatelli[22], Valeria Capra[23], Jacob O. Kitzman[3], Miriam H. Meisler[3,*]

ARTICLE INFO

*Article history:*
Received 2 August 2023
Received in revised form
31 January 2024
Accepted 1 February 2024
Available online 5 February 2024

*Keywords:*
SLC12A9
Co-transporter
Lysosome
Neurodevelopmental disorder
Osmoregulation

ABSTRACT

**Purpose:** Pathogenic variants of *FIG4* generate enlarged lysosomes and neurological and developmental disorders. To identify additional genes regulating lysosomal volume, we carried out a genome-wide activation screen to detect suppression of enlarged lysosomes in *FIG4*$^{-/-}$ cells.
**Methods:** The CRISPR-a gene activation screen utilized sgRNAs from the promoters of protein-coding genes. Fluorescence-activated cell sorting separated cells with correction of the enlarged lysosomes from uncorrected cells. Patient variants of *SLC12A9* were identified by exome or genome sequencing and studied by segregation analysis and clinical characterization.
**Results:** Overexpression of *SLC12A9*, a solute co-transporter, corrected lysosomal swelling in *FIG4*$^{-/-}$ cells. SLC12A9 (NP_064631.2) colocalized with LAMP2 at the lysosome membrane. Biallelic variants of *SLC12A9* were identified in 3 unrelated probands with neurodevelopmental disorders. Common features included intellectual disability, skeletal and brain structural abnormalities, congenital heart defects, and hypopigmented hair. Patient 1 was homozygous for nonsense variant p.(Arg615*), patient 2 was compound heterozygous for p.(Ser109Lysfs*20) and a large deletion, and proband 3 was compound heterozygous for p.(Glu290Glyfs*36) and p.(Asn552Lys). Fibroblasts from proband 1 contained enlarged lysosomes that were corrected by wild-type *SLC12A9* cDNA. Patient variant p.(Asn552Lys) failed to correct the lysosomal defect.
**Conclusion:** Impaired function of SLC12A9 results in enlarged lysosomes and a recessive disorder with a recognizable neurodevelopmental phenotype.



The Article Publishing Charge (APC) for this article was paid by NIH GM24872.

Andrea Accogli and Young N. Park contributed equally.

*Correspondence and requests for materials should be addressed to Miriam Meisler, Department of Human Genetics, University of Michigan, 4808 Medical Sciences II, Ann Arbor, MI 48109-5618. *Email address:* meislerm@umich.edu

Affiliations are at the end of the document.

doi: https://doi.org/10.1016/j.gim.2024.101097

## Introduction

The signaling lipid PI(3,5)$P_2$ regulates ion channels and transporters localized in the lysosomal membrane.[1] PI(3,5)$P_2$ is synthesized by an evolutionarily conserved protein complex that includes the lipid phosphatase FIG4, the kinase PIKFYVE, and the scaffold protein VAC14.[2] Loss of FIG4 destabilizes the complex and reduces PI(3,5)$P_2$ abundance, resulting in enlarged lysosomes, as well as defective autophagy.[3,4] Partial and complete loss-of-function variants of FIG4 result in the recessive peripheral neuropathy Charcot-Marie-Tooth type 4J [MIM: 611228][3,5] and the Yunis-Varón Syndrome [MIM: 216340].[6]

FIG4 null cells in culture exhibit extensive vacuolization, with accumulation of enlarged, translucent membrane-bounded vesicles that are positive for lysosomal membrane markers.[3,7] FIG4 null cells are deficient in PI(3,5)$P_2$, which regulates the activity of the ion transporters TPC1, TPC2, TRPML1, and CLCN7.[1,8,9] Loss of function of yeast FIG4 likewise reduces PI(3,5)$P_2$ and results in swelling of the vacuole.[1] These observations support the view that elevated osmotic pressure contributes to lysosome swelling in FIG4 null cells. We sought to identify additional genes involved in regulation of lysosome volume with a genome-wide screen.

## Material and Methods

Full methodology detailing the genome-wide suppressor screen, genetic analysis, plasmid vectors, and cell culture and transfection conditions are provided in Supplemental Materials and Methods.

For the suppressor screen, the accessory factors dCas9-VP64 and MS2-p65-HSF1[10] were stably integrated into a *FIG4*$^{-/-}$ HAP1 cell line, which was then transfected with the synergistic activation mediator library containing 6 sgRNA clones per promoter region −200 to +1 for >19,000 protein-coding genes.[11] Transduced cells expressing the sgRNA vector were selected using blasticidin. *FIG4*$^{-/-}$ cells with small, corrected lysosomes were separated from cells with enlarged lysosomes by fluorescence-activated cell sorting based on intensity of staining with LysoTracker DND 160 as described.[7] sgRNAs were sequenced from the initial and final populations to identify genes enriched in the corrected population.

## Results

### Identification of SLC12A9 in a genome-wide screen

We carried out a genome-wide suppressor screen for genes that could reduce the hyperosmotic swelling in *FIG4*$^{-/-}$ cells. Deep sequencing of the integrated sgRNAs from the rescued, non-vacuolated population revealed that *SLC12A9* sgRNAs were significantly enriched compared with baseline ($\log_2$ = 2.0; FDR adjusted $P = 1 \times 10^{-9}$). Vacuole suppression by *SLC12A9* (HGNC:17435) was confirmed by transfection of FIG4 null HAP1 cells with tagged wild-type *SLC12A9* cDNA. The non-transfected *FIG4*$^{-/-}$ cells were 53% vacuolated (234/436 cells), whereas transfection with the cDNA rescued vacuolization phenotype to 14% (54/391 cells) (Figure 1B and C) ($X^2 = 139$, $P < .001$). The myc-tagged wild-type SLC12A9 protein colocalized with the lysosomal membrane protein LAMP2 in transfected HAP1 cells (Figure 1D). A similar perinuclear concentration of lysosomes was seen in nontransfected HAP1 cells (Figure 1E).

*SLC12A9* is a member of the solute co-transporter gene family[13] that encodes a protein of 914 amino acid residues (NP 064631.2) with 12 predicted transmembrane segments and a cytoplasmic C-terminal domain. The amino acid sequence contains 2 lysosomal importation motifs (D/E XX(X)LL) beginning at residues 4 and 325, as well as 4 YXXØ motifs.

### Identification of biallelic variants of *SLC12A9*

Because variants of *SLC12A9* were not previously associated with a human disorder, we queried *SLC12A9* in the Matchmaker Exchange platform GeneMatcher,[14] screened the public databases DECIPHER,[15] LOVD,[16] and Geno2MP and examined 4 genomic data sets of rare undiagnosed pediatric neurodevelopmental disorders containing exome and genome data of more than 100,000 families. We identified 3 unrelated probands with biallelic variants in *SLC12A9* (NM_020246.4) displaying neurodevelopmental phenotypes with overlapping clinical features. Each patient was evaluated by expert pediatricians, neurologists, and geneticists at the referring centers and clinical charts and neuroimaging scans were reviewed for deep phenotype analysis.

Pedigrees of 3 families segregating biallelic variants are shown in Figure 2A.

In family 1, trio exome sequencing identified the homozygous nonsense variant NM_020246.4:c.1843C>T p.(Arg615*) in the proband while parents were heterozygous. This rare variant is present in 49 heterozygotes in the gnomAD database version 4, minor allele frequency of $3.4 \times 10^{-5}$ but not in homozygote state. There is no known history of consanguinity in the family.

In family 2, genome sequencing of the proband detected the *SLC12A9* frameshift variant NM_020246.4:c.325dup p.(Ser109Lysfs*20) that was inherited from the unaffected mother. This variant is present in 1 individual in the gnomAD database version 4. Analysis of the genome sequence for large deletions identified a 2.1 Mb de novo deletion ((98,261,637-100,363,719)x1 [GRCh37]) on chromosome 7q22.1 that fully encompasses *SLC12A9*. The deletion was confirmed by a microarray and found to be in trans with the *SLC12A9* frameshift variant (Supplemental Figure 1).

In family 3, trio exome sequencing identified compound heterozygosity for the *SLC12A9* frameshift variant NM_020246.4:c.866_867insT p.(Glu290Glyfs*36), and the missense variant NM_020246.4:c.1656C>A p.(Asn552Lys). This frameshift variant is present in heterozygous state in 62 individuals in gnomAD version 4, allele frequency $3.8 \times 10^{-5}$. The missense variant changes an evolutionarily conserved asparagine, residue 552, that is conserved in vertebrate, invertebrate and yeast genes (Figure 1J). This variant is predicted to be deleterious by multiple in silico tools, with a Rare Exome Variant Ensemble Learner (REVEL) score of 0.7[17] and a Combined Annotation Dependent Depletion (CADD) score of 24.0.[18]

Sanger sequencing confirmed segregation of the variants with the phenotype in all 3 families. Patients 1 and 3 did not harbor pathogenic or likely pathogenic variants in other Online Mendelian Inheritance in Man genes. The 7q22.1 deletion in patient 2 does not appear to include Online Mendelian Inheritance in Man morbid genes that are likely to contribute to the phenotype by haploinsufficiency (Supplemental Table 1).

## Clinical features of individuals with biallelic *SLC12A9* variants

Clinical features are summarized in Supplemental Table 2.

Patient 1 was born preterm at 29 + 3 weeks gestation after an uneventful pregnancy. Neonatal course was complicated by respiratory distress at birth and an atrium septum defect and patent ductus arteriosus that closed spontaneously. The first years of life were remarkable for hypotonia, failure to thrive, and severe motor and language delay that led to a diagnosis of moderate intellectual disability (ID). He had 1 febrile seizure at the age of 18 months. Brain MRI showed reduced white matter volume with a thin corpus callosum associated with hypoplasia of the pons and inferior cerebellar vermis (Figure 2C-I). Skeletal survey and spinal MRI revealed fusion and segmentation vertebral defects causing scoliosis, including C2-C3 fusion, butterfly vertebrae in D3 and D7, and fused hemivertebra in L2 (Figure 2II-IV). There were 11 thoracic vertebrae with corresponding ribs bilaterally. In addition, he had a filar lipoma tethered the cord at level L3-L4 (Figure 2III). He was found to have retinal depigmentation of the right eye at ophthalmological evaluation. At 9 years and 10 months of age, he was found to have short stature, microcephaly, light blond hair, eyebrows and eyelashes, aplasia cutis on the vertex, brachycephaly, long face, upslanting palpebral fissures, clinodactyly of the 5$^{th}$ finger bilaterally, hallux valgus and toes reducible contractures (Figure 2B).

Patient 2 was prenatally diagnosed with a complex congenital heart disease consisting of complete atrioventricular canal defect Rastelli A, predominance of the right ventricle, and aortic coarctation. He underwent surgical cardiac correction at birth followed by 2 further interventions within first 3 years of life with favorable cardiac function outcome. Head CT at the age of 5 months showed brachycephaly with patent sutures and extensive cranial lacunae (Figure 2D-I-II). There was moderate enlargement of the fronto-temporal subarachnoid spaces and hypoplasia of the pons and inferior cerebellar vermis (Figure 2III-IV). His first years of life were also remarkable for hypotonia, severe global developmental delay, significant speech delay and stereotypical hand movements that led to a diagnosis of moderate ID and autism spectrum disorder. He had light blond hair, eyebrows, and eyelashes since birth. At the last evaluation at the age of 13 years and 2 months, he was found to have short stature, mild microcephaly and brachycephaly, right ptosis, upslanting palpebral fissures, telecanthus, depressed nasal bridge, short nose with broad nasal tip, prominent super incisors and full cheeks, and bilateral V finger camptodactyly (Figure 2B).

Patient 3 was a female with history of hypotonia, failure to thrive, infantile spasms, and myoclonic and tonic seizures since infancy that required multiple anti-seizure medications. She was never able to sit, walk, or say any words. Brain MRI showed delayed myelination with mild reduction of white matter volume, enlargement of the frontal subarachnoid spaces, and enlargement of the frontal subarachnoid spaces and mild pontine hypoplasia (Figure 2EI-III). An echocardiogram revealed an atrium septum defect that closed spontaneously. At the last evaluation at 6 years and 3 months, she had thin white hair, eyelashes and eyebrows, frontal bossing, left eye strabismus, small ears with overfolded helix, full cheeks, dysplastic teeth, and livedo reticularis (Figure 2B). The patient passed away at the time of last evaluation because of pneumonia complicated by macrophage activation syndrome.

## Cellular phenotypes of SLC12A9 deficiency

In view of the rescue of lysosomal vacuolization by *SLC12A9* in the genome-wide screen, we examined the cellular phenotype caused by deficiency of SLC12A9. Skin fibroblasts from patient 1, homozygous for the nonsense variant p.(Arg615*), were examined by phase contrast microscopy. The cytoplasm of the patient fibroblasts was filled with vacuoles (96% of cells, $n = 302$) (Figure 1F). Vacuoles are absent in wildtype fibroblasts (3% of cells, $n = 300$; $X^2 = 511$, <0.001, $\chi^2$ test) (Figure 1F and G). Transfection with wild-type *SLC12A9* cDNA reduced vacuolization of patient fibroblasts to 15% (70/483) ($X^2 = 498$, <0.001) (Figure 1G and H). Thus, the *SLC12A9* variant p.(Arg615*) is responsible for vacuolization that is corrected by wild-type *SLC12A9*.

The membrane of the enlarged vacuoles was positive for LAMP2, indicative of lysosomal origin (Figure 1I). These enlarged lysosomes were not present in the wild-type human fibroblasts (Figure 1H). The enlarged vesicles in patient fibroblasts closely resembles the FIG4 null cells in Figure 1A and the recently described *SLC12A9* knockout in a macrophage cell line (Levin-Konigsberg R, Mitra K, Nigam A, et al. posted as a preprint on bioRxiv.org on May 22, 2023.

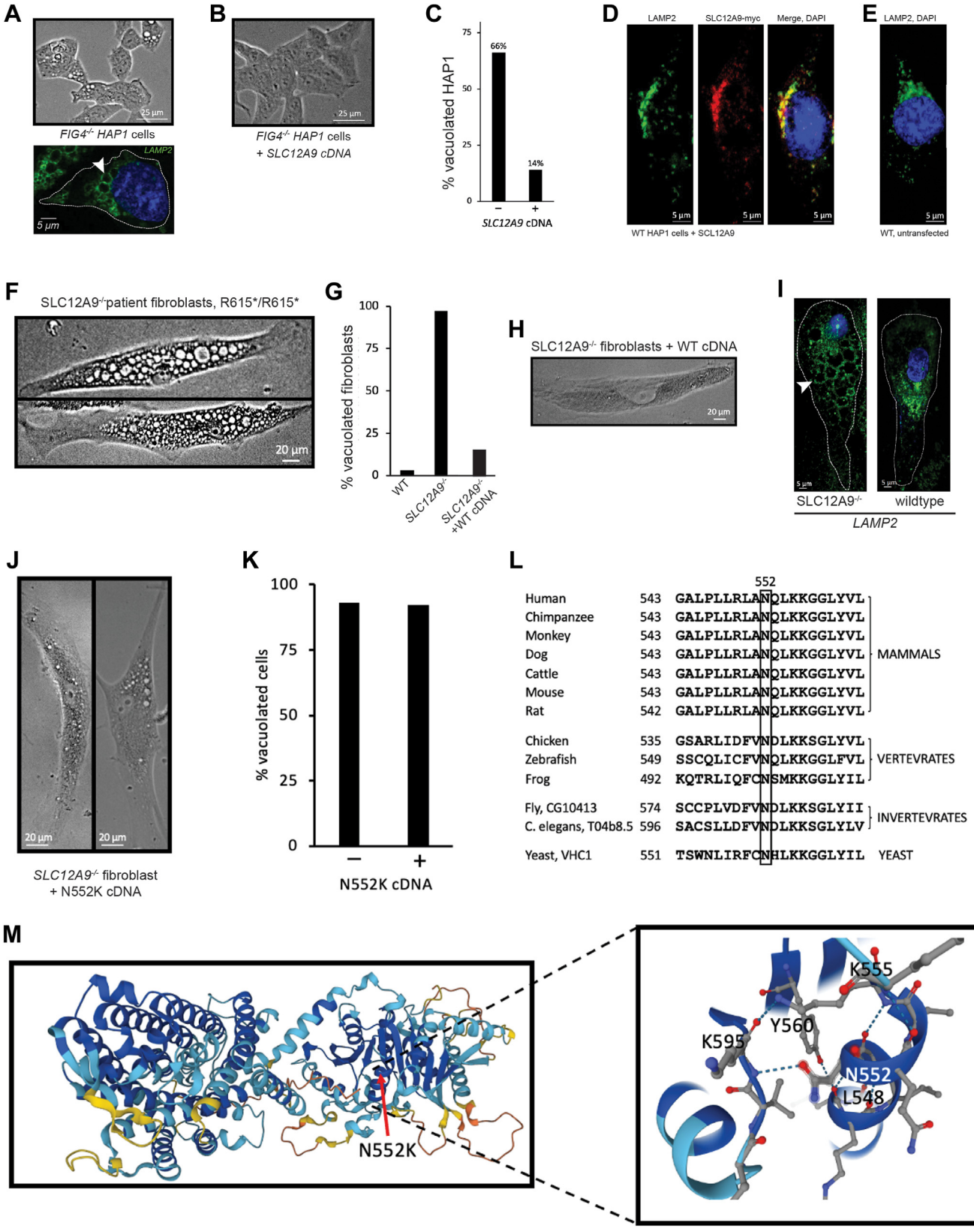


**Figure 1** **Enlarged lysosomes in *SLC12A9* mutant cells.** A. FIG4 null human HAP1 cells contain enlarged, lysosome-derived vacuoles that are immunostained for lysosomal membrane protein LAMP2 (arrowhead) with Abcam antibody ab25631. B. Rescue of vacuoles by transfection of FIG4 null HAP1 cells with wild-type *SLC12A9* cDNA (Origene RC213861). Non-transfected control cells were not corrected (not shown). C. Quantitation of vacuoles in FIG4 null HAP1 cells in the presence and absence of SLC12A9 cDNA. D. Colocalization of SLC12A9 (red) with lysosomal membrane marker LAMP2 (green) in wild-type HAP1 cells. SLC12A9 was myc-tagged at the C terminus

doi: https://doi.org/10.1101/2023.05.22.541801), suggesting a related mechanism.

## Impaired function of missense variant p.(Asn552Lys)

The substitution of lysine residue 552 of SLC12A9 by asparagine is predicted to disrupt a hydrogen bond in the cytoplasmic domain of the protein (Figure 1M). To test the functional consequence of p.(Asn552Lys) in proband 3, we carried out site-directed mutagenesis of the *SLC12A9* cDNA to introduce the lysine substitution at reside 552 and tested the ability of the mutated cDNA to rescue the enlarged lysosomes in fibroblasts from patient 1. Transfection with the p.(Asn552Lys) cDNA did not rescue vacuolization (Figure 1J and K) (175/192 cells vacuolated) compared with 186 of 202 cells vacuolated without the cDNA) ($X^2 = 0.33$, $P = .56$). This variant thus lacks activity in the functional assay.

## Discussion

*SLC12A9* was identified in our genome-wide screen by correction of the enlarged lysosomes in cells with loss of function of FIG4. SLC12A9 was recently shown to co-transport ammonium and chloride ions from the lysosomal lumen to the cytoplasm (Levin-Konigsberg R, Mitra K, Nigam A, et al. posted as a preprint on bioRxiv.org on May 22, 2023. doi: https://doi.org/10.1101/2023.05.22.541801). This process also involves efflux of $Na^+$ from lysosomes via TPC channels[19] and efflux of chloride via the transporter TMEM206.[20] This functional role of SLC12A9 suggests that overexpression could directly relieve hyperosmotic lysosomes in FIG4-null cells by allowing escape of cations from the lysosomal lumen. There are interesting similarities in the phenotypes that result from deficiency of FIG4 and SLC12A9, including neurological impairment and skeletal defects. Variants of mouse *Fig4* also cause neuronal degeneration, myelination defects, diluted pigmentation, and skeletal abnormalities.[2,3,6]

The 6 patient alleles of *SLC12A9* are predicted to act with a loss-of-function mechanism, leading to a neurodevelopmental disorder characterized by hypotonia, failure to thrive, moderate to severe developmental delay and ID, pale hair, eyebrows and eyelashes, and variable presence of seizures, congenital heart defects, skeletal, and brain abnormalities. The combination of these features could alert clinicians to recognize this novel neurodevelopmental disorder in the clinical setting.

*SLC12A9* has a pLI value of 0 in the gnomAD population database, indicating that there is no strong evidence of haploinsufficiency for this gene. There are no homozygous loss-of-function variants of *SLC12A9* in gnomAD or BRAVO databases of healthy/non-severely affected individuals (last accessed 12 November 2023), consistent with a detrimental effect of homozygous loss-of-function alleles. *SLC12A9* is also predicted to be associated with a recessive condition by a linear discriminant analysis score of −0.717, where a score of <0.02 corresponds to "very likely recessive" according to the DOMINO algorithm.[21] These observations and the overlapping phenotypes in the 3 unrelated individuals with biallelic variants indicate that *SLC12A9* is a strong candidate gene for a novel neurodevelopmental disorder.

*SLC12A9* is abundantly expressed in the central nervous system, with highest expression in corpus callosum and white matter (Supplemental Figure 2). In 2 patients with SLC12A9 deficiency we noted reduced white matter volume and thin corpus callosum, associated with delayed myelination for one of them. Additional cases will be required to determine whether hypomyelination is a consistent feature of *SLC12A9* related disorders.[6,22] Other nonspecific brain abnormalities in the present series include mild reduction of cerebral volume with enlargement of subarachnoid spaces and hypoplasia of the pons and inferior cerebellar vermis.

Diluted hair pigmentation was observed in all 3 probands, mirroring that of patients with several lysosomal disorders, as well as FIG4 deficiency[6] and the Fig4 null mouse.[3,23] Patient 1 also had retinal depigmentation. Common variation near *SLC12A9* associates with hair color[24] and *SLC12A9* emerged as a top hit in a genome-wide CRISPR screen for genes necessary for normal melanin levels in a cultured pigment cell model.[25] In *Fig4* null mice, diluted pigmentation is caused by impaired maturation of the structural protein PMEL in melanosomes, lysosome-derived organelles.[23]

The data presented here associate *SLC12A9* with a role in lysosome function, likely related to osmoregulation. The evolutionary relationship of *SLC12A9* to the *SLC12* family of chloride cation co-transporters and its protective effect in FIG4 null cells support a role in lysosomal ion flux. This hypothesis is further supported by the proteomic detection

and detected with Abcam antibody ab206486. Quantitation of colocalization[12] gave Manders Coefficients MCC1 = 0.836 and MCC2 = 0.816. E. Nontransfected wild-type HAP1 control. F. Fibroblasts from Patient 1 contain enlarged vacuoles similar to the FIG4 null cells in (A). G. Quantitation of cells containing vacuoles in fibroblasts from patient 1 and rescue by transfection with wild-type *SLC12A9* cDNA. H. Transfection of patient 1 fibroblasts with wild-type SLC12A9 cDNA rescues vacuoles. I. The enlarged vacuoles in fibroblasts from patient 1 stain for the lysosomal membrane marker LAMP2 (arrowhead). J. Missense variant p.Asn552Lys cDNA does not rescue vacuolization in patient 1 *SLC12A9* fibroblasts. Patient fibroblasts were transfected with *SLC12A9*-Asn552Lys cDNA. K. Quantitation of vacuolated patient fibroblasts transfected with p.(Asn552Lys) cDNA. L. Arginine residue 552 is evolutionarily conserved in potassium-chloride co-transporters. M. Variant p.(Asn552Lys) is located at the end of an a-helix in the predicted cytoplasmic domain of SLC12A9. The hydrogen bond between residues Asn552 and Lys595 in the wild-type protein is predicted to be disrupted by the substitution Lys552.

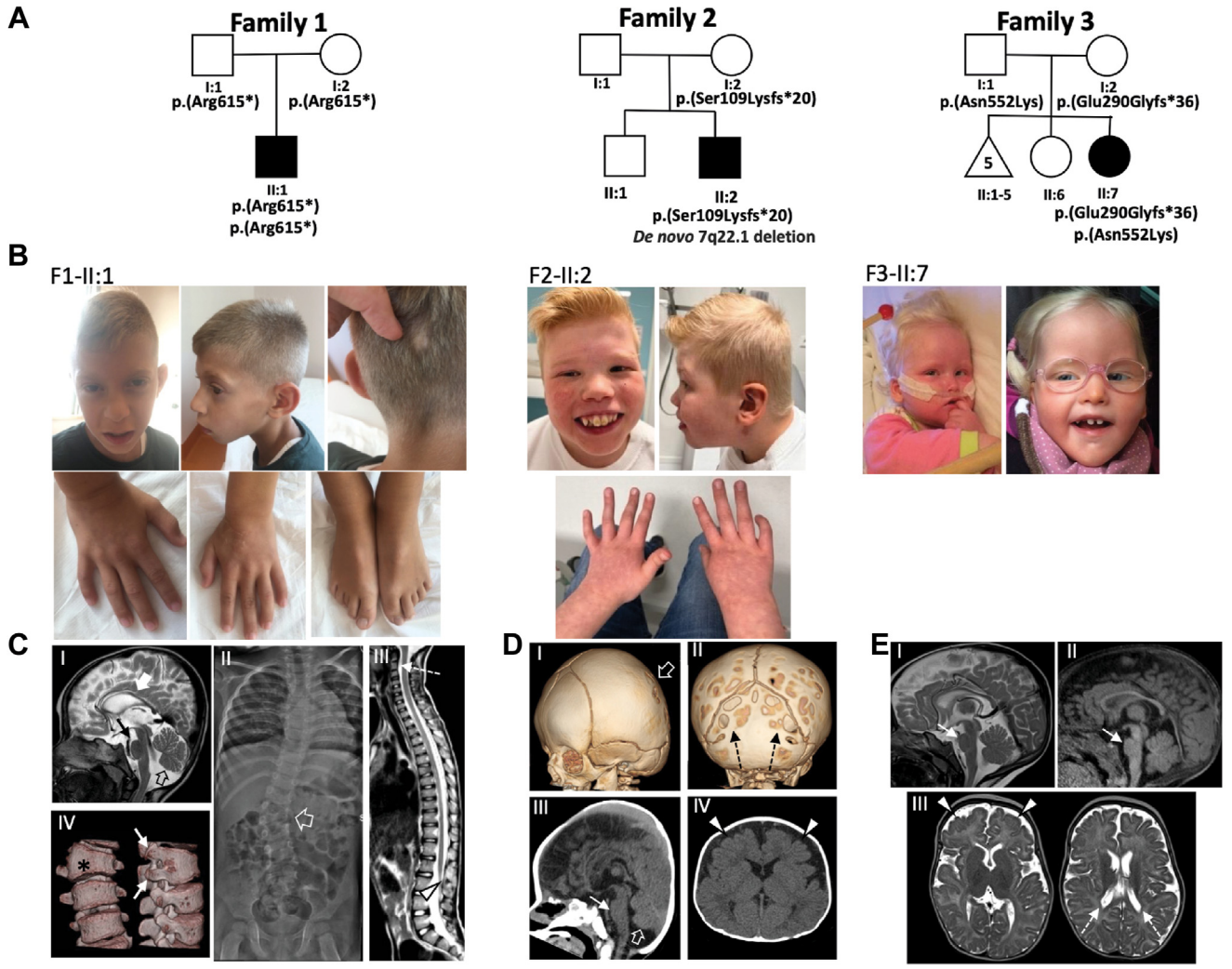


**Figure 2 Pedigrees and clinical imaging of individuals with biallelic *SLC12A9* variants.** A. Pedigrees of 3 probands. Segregation of variants was confirmed by Sanger sequencing. B. Facial and hand photographs and (C) skeletal and brain imaging of individuals with biallelic *SLC12A9* variants. Very light blond/white hair, eyebrows and eyelashes are present in all individuals. Patient 1 has long face, whereas patient 2 and 3 have full cheeks. Additional features for patient 1 include aplasia cutis on the vertex, upslanting palpebral fissures, long philtrum, abnormal earlobe shape, clinodactyly of the 5$^{th}$ finger bilaterally, hallux valgus, and toes reducible contractures. Patient 2 presents with right ptosis, upslanting palpebral fissures, telecanthus, depressed nasal bridge, short nose with broad nasal tip, prominent super incisors, bilateral V finger camptodactyly, and livedo reticularis. Patient 3 displays frontal bossing, left eye strabismus, small ears with overfolded helix, and livedo reticularis. Brain and skeletal findings of patient 1 (C, I-IV), patient 2 (D, I-IV), and patient 3 (E, I-III). C-I. Brain MRI with sagittal T2-weighted image reveals thin corpus callosum (white thick arrow), hypoplasia of the pons (black thin arrow), and of the inferior cerebellar vermis (black empty arrow). C-II. Spinal X-ray, frontal view, shows right thoraco-lumbar convex scoliosis due to a L2 fused hemivertebra (empty arrow). Note that there are 11 ribs bilaterally. C-III. Spinal MRI with sagittal T2-weighted image demonstrates C2-C3 fusion and a low-lying conus terminating at L2-L3 level (arrowhead). C-IV. Spinal CT, 3D reconstruction, better depicts the L2 fused hemivertebra (asterisk) with 2 right-sided vertebral peduncles (thin arrows). D-I. Head CT with 3D reconstructions (I, II) show brachycephaly (empty arrow) and diffuse cranial lacunae (dashed arrows) with patent cranial sutures. Sagittal (III) and axial (IV) head CT reformatting reveal a small pons (thin arrow) associated with hypoplasia of the inferior cerebellar vermis (empty arrow) and enlarged fronto-temporal subarachnoid spaces (arrowheads). E. Brain MRI performed at 5 months of age with sagittal T2-weighted (I) and T1-weighted (II) images demonstrate hypoplasia of the pons (thin arrows). III. Axial T2-weighted images show enlargement of the frontal subarachnoid spaces (arrowheads), mild volume reduction of the periventricular white matter (dashed arrows), and delayed myelination.

of SLC12A9 in purified lysosome membranes[26] and the recent direct demonstration of co-transport of ammonium and chloride ions out of lysosomes (Levin-Konigsberg R, Mitra K, Nigam A, et al. posted as a preprint on bioRxiv.org on May 22, 2023. doi: https://doi.org/10.1101/2023.05.22.541801). In summary, our work identifies a novel neurodevelopmental disorder caused by deficiency of SLC12A9, expanding the list of neurogenetic conditions caused by defective lysosomal membrane proteins.[27] Further studies with iPSC-derived cerebral neurons and

organoids and knockout animal models may shed light on the mechanisms leading to impaired brain development and function in patients with SLC12A9 deficiency.

## Data Availability

Human variant data included in this study will be deposited in ClinVar before publication.

## Acknowledgments

The authors are grateful to the patients and families who participated in this investigation. The authors thank Xu Cao, PhD, for helpful discussions. The authors acknowledge the Telethon Undiagnosed Disease Program (TUDP) for exome sequencing of family 1 within Telethon project GSP15001. The human CRISPR 2-plasmid activation pooled library (SAM) was available through Addgene (library #1000000078).

## Funding

Supported by NIH Grant R01 GM24872 to MHM. K.F. is supported by KULeuven BOF grant C14/19/096, FWO grant G072921N and an unrestricted research grant from Swedish Orphan Biovitrum AB (Sobi).

## Author Information

Conceptualization: A.A., M.H.M., J.O.K., Y.N.P., G.M.L.; Formal analysis: A.A., Y.N.P., G.M.L., M.H.M.; Investigation: J.D., M.H., V.L., V.C., V.S., Y.N.P., G.M.L., A.A., D.L., A.T., V.N., E.T. K.F.; Supervision: A.A., M.H.M.; Visualization: A.A., Y.N.P., G.M.L., M.Severino; Writing-original draft: A.A, M.H.M.; Writing-review and editing: A.A., Y.N.P., G.M.L., M.Severino, M.Scala, J.D., M.H., D.L., F.K., V.S., P.d.M., S.G., A.T., V.N., M.Srour, E.T., V.L., K.F., G.P., V.C., J.O.K., M.H.M.

## Ethics Declaration

The study was approved by the institutional ethics committees of the participating centers and written informed consent was obtained from the families involved in this study, including permission to publish photographs, in accordance with the Declaration of Helsinki. All experimental work was performed in accordance with University of Michigan institutional guidelines and regulations.

## Conflict of Interest

The authors declare no conflicts of interest.

## Additional Information

The online version of this article (https://doi.org/10.1016/j.gim.2024.101097) contains supplemental material, which is available to authorized users.

## Affiliations

[1]Division of Medical Genetics, Department of Specialized Medicine, McGill University Health Centre (MUHC), Montreal, QC, Canada; [2]Department of Human Genetics, McGill University, Montreal, QC, Canada; [3]Department of Human Genetics, University of Michigan, Ann Arbor, MI; [4]Neuroradiology Unit, IRCCS Istituto Giannina Gaslini, Genoa, Italy; [5]Department of Neurosciences, Rehabilitation, Ophthalmology, Genetics, Maternal and Child Health, Università Degli Studi di Genova, Genoa, Italy; [6]Pediatric Neurology and Muscular Diseases Unit, IRCCS Istituto Giannina Gaslini, Genoa, Italy; [7]University Children's Hospital, University Medical Center Hamburg Eppendorf, Hamburg, Germany; [8]Institute of Human Genetics, University Medical Center Hamburg-Eppendorf, Hamburg, Germany; [9]Department of Neuromuscular Disorders, Queen Square Institute of Neurology, University College London, London, United Kingdom; [10]Department of Biotechnological and Applied Clinical Sciences, University of L'Aquila, 67100, L'Aquila, Italy; [11]UOC Genetica Medica, IRCCS G. Gaslini, Genoa, Italy; [12]Telethon Institute of Genetics and Medicine (TIGEM), Naples, Italy; [13]Department of Precision Medicine, University of Campania "Luigi Vanvitelli", Naples, Italy; [14]Department of Pediatrics, Division of Pediatric Neurology, McGill University, Montreal, QC, Canada; [15]McGill University Health Center (MUHC) Research Institute, Montreal, QC, Canada; [16]Montreal Neurological Institute, McGill University, Montreal, QC, Canada; [17]Department of Genetics and Genomic Sciences, Icahn School of Medicine at Mount Sinai, New York, NY; [18]Mindich Child Health and Development Institute, Icahn School of Medicine at Mount Sinai, New York, NY; [19]Charles Bronfman Institute for Personalized Medicine, Icahn School of Medicine at Mount Sinai, New York, NY; [20]Center for Molecular and Vascular Biology, Department of Cardiovascular Sciences, University of Leuven, Leuven, Belgium; [21]Paediatric Hemato-Oncology, University Hospitals Leuven, Leuven, Belgium; [22]Department of Neurosurgery, Gaslini Children's Hospital, Genoa, Italy; [23]Genomics and Clinical Genetics, IRCCS Instituto G. Gaslini, Genoa, Italy

## Web resources

https://gnomad.broadinstitute.org/
https://www.deciphergenomics.org/
https://www.lovd.nl/
https://geno2mp.gs.washington.edu/Geno2MP/#/
https://bravo.sph.umich.edu/freeze8/hg38/
https://www.ukbiobank.ac.uk/
https://www.genomicsengland.co.uk/
https://www.proteinatlas.org/ENSG00000146828-SLC12A9/tissue

## References


1. Rivero-Ríos P, Weisman LS. Roles of PIKfyve in multiple cellular pathways. *Curr Opin Cell Biol*. 2022;76:102086. http://doi.org/10.1016/j.ceb.2022.102086
2. Jin N, Chow CY, Liu L, et al. VAC14 nucleates a protein complex essential for the acute interconversion of PI3P and PI(3,5)P(2) in yeast and mouse. *EMBO J*. 2008;27(24):3221-3234. http://doi.org/10.1038/emboj.2008.248
3. Chow CY, Zhang Y, Dowling JJ, et al. Mutation of FIG4 causes neurodegeneration in the pale tremor mouse and patients with CMT4J. *Nature*. 2007;448(7149):68-72. http://doi.org/10.1038/nature05876
4. Ferguson CJ, Lenk GM, Jones JM, et al. Neuronal expression of Fig4 is both necessary and sufficient to prevent spongiform neurodegeneration. *Hum Mol Genet*. 2012;21(16):3525-3534. http://doi.org/10.1093/hmg/dds179
5. Nicholson G, Lenk GM, Reddel SW, et al. Distinctive genetic and clinical features of CMT4J: a severe neuropathy caused by mutations in the PI(3,5)$P_2$ phosphatase FIG4. *Brain*. 2011;134(7):1959-1971. http://doi.org/10.1093/brain/awr148
6. Campeau PM, Lenk GM, Lu JT, et al. Yunis-Varón syndrome is caused by mutations in FIG4, encoding a phosphoinositide phosphatase. *Am J Hum Genet*. 2013;92(5):781-791. http://doi.org/10.1016/j.ajhg.2013.03.020
7. Lenk GM, Park YN, Lemons R, et al. CRISPR knockout screen implicates three genes in lysosome function. *Sci Rep*. 2019;9(1):9609. http://doi.org/10.1038/s41598-019-45939-w
8. Cao X, Lenk GM, Mikusevic V, Mindell JA, Meisler MH. The chloride antiporter CLCN7 is a modifier of lysosome dysfunction in FIG4 and VAC14 mutants. *PLoS Genet*. 2023;19(6):e1010800. http://doi.org/10.1371/journal.pgen.1010800
9. Leray X, Hilton JK, Nwangwu K, et al. Tonic inhibition of the chloride/proton antiporter ClC-7 by PI(3,5)P2 is crucial for lysosomal pH maintenance. *Elife*. 2022;11:e74136. http://doi.org/10.7554/eLife.74136
10. Joung J, Engreitz JM, Konermann S, et al. Genome-scale activation screen identifies a lncRNA locus regulating a gene neighbourhood. *Nature*. 2017;548(7667):343-346. http://doi.org/10.1038/nature23451
11. Konermann S, Brigham MD, Trevino AE, et al. Genome-scale transcriptional activation by an engineered CRISPR-Cas9 complex. *Nature*. 2015;517(7536):583-588. http://doi.org/10.1038/nature14136
12. Bolte S, Cordelières FP. A guided tour into subcellular colocalization analysis in light microscopy. *J Microsc*. 2006;224(3):213-232. http://doi.org/10.1111/j.1365-2818.2006.01706.x
13. Chew TA, Orlando BJ, Zhang J, et al. Structure and mechanism of the cation–chloride cotransporter NKCC1. *Nature*. 2019;572(7770):488-492. http://doi.org/10.1038/s41586-019-1438-2
14. Sobreira N, Schiettecatte F, Valle D, Hamosh A. GeneMatcher: a matching tool for connecting investigators with an interest in the same gene. *Hum Mutat*. 2015;36(10):928-930. http://doi.org/10.1002/humu.22844
15. Firth HV, Richards SM, Bevan AP, et al. DECIPHER: database of chromosomal imbalance and phenotype in humans using Ensembl resources. *Am J Hum Genet*. 2009;84(4):524-533. http://doi.org/10.1016/j.ajhg.2009.03.010
16. Fokkema IF, Taschner PE, Schaafsma GC, Celli J, Laros JF, den Dunnen JT. LOVD v.2.0: the next generation in gene variant databases. *Hum Mutat*. 2011;32(5):557-563. http://doi.org/10.1002/humu.21438
17. Ioannidis NM, Rothstein JH, Pejaver V, et al. REVEL: an ensemble method for predicting the pathogenicity of rare missense variants. *Am J Hum Genet*. 2016;99(4):877-885. http://doi.org/10.1016/j.ajhg.2016.08.016
18. Rentzsch P, Witten D, Cooper GM, Shendure J, Kircher M. CADD: predicting the deleteriousness of variants throughout the human genome. *Nucleic Acids Res*. 2019;47(D1):D886-D894. http://doi.org/10.1093/nar/gky1016
19. Freeman SA, Uderhardt S, Saric A, et al. Lipid-gated monovalent ion fluxes regulate endocytic traffic and support immune surveillance. *Science*. 2020;367(6475):301-305. http://doi.org/10.1126/science.aaw9544
20. Zeziulia M, Blin S, Schmitt FW, Lehmann M, Jentsch TJ. Proton-gated anion transport governs macropinosome shrinkage. *Nat Cell Biol*. 2022 June;24(6):885-895. http://doi.org/10.1038/s41556-022-00912-0
21. Quinodoz M, Royer-Bertrand B, Cisarova K, Di Gioia SA, Superti-Furga A, Rivolta C. DOMINO: using machine learning to predict genes associated with dominant disorders. *Am J Hum Genet*. 2017;101(4):623-629. http://doi.org/10.1016/j.ajhg.2017.09.001
22. Winters JJ, Ferguson CJ, Lenk GM, et al. Congenital CNS hypomyelination in the Fig4 null mouse is rescued by neuronal expression of the PI(3,5)P(2) phosphatase FIG4. *J Neurosci*. 2011;31(48):17736-17751. http://doi.org/10.1523/JNEUROSCI.1482-11.2011
23. Bissig C, Croisé P, Heiligenstein X, et al. The PIKfyve complex regulates the early melanosome homeostasis required for physiological amyloid formation. *J Cell Sci*. 2019;132(5):jcs229500. http://doi.org/10.1242/jcs.229500
24. Morgan MD, Pairo-Castineira E, Rawlik K, et al. Genome-wide study of hair colour in UK Biobank explains most of the SNP heritability. *Nat Commun*. 2018;9(1):5271. http://doi.org/10.1038/s41467-018-07691-z
25. Bajpai VK, Swigut T, Mohammed J, et al. A genome-wide genetic screen uncovers novel determinants of human pigmentation. *Science*. 2023;381(6658):eade6289. http://doi.org/10.1126/science.eade6289
26. Chapel A, Kieffer-Jaquinod S, Sagné C, et al. An extended proteome map of the lysosomal membrane reveals novel potential transporters. *Mol Cell Proteomics*. 2013;12(6):1572-1588. http://doi.org/10.1074/mcp.M112.021980
27. Deneubourg C, Ramm M, Smith LJ, et al. The spectrum of neurodevelopmental, neuromuscular and neurodegenerative disorders due to defective autophagy. *Autophagy*. 2022;18(3):496-517. http://doi.org/10.1080/15548627.2021.1943177